Parallel Magnetic Resonance Imaging

Ulrich Katscher and Peter Börnert

Philips Research Laboratories, Roentgenstrasse 24-26, D-22335 Hamburg, Germany

Summary: Parallel MRI started with the introduction of coil arrays in improving radiofrequency (RF) acquisition (what is called *parallel imaging*) and continued with an analogous development for RF transmission (*parallel transmission*). Based on differences in the spatial sensitivity distributions of the involved array elements, both techniques try to shorten the respective *k*-space trajectory. Parallel imaging refers to the acquisition of *k*-space data, whereas parallel transmission is dealing with the deposition of RF energy packages in the excitation *k*-space. However, parallel transmission is not simply the reciprocal of parallel imaging. The main goal of parallel imaging is the shortening of the acquisition time. The main goal of parallel transmission is the shortening of the pulse duration of spatially selective RF pulses. The present article describes the basic concept, the state of the art, and the similarities and differences of both technologies. **Key Words:** Magnetic resonance imaging, parallel imaging, parallel transmission, RF coil array, RF pulses, inverse problem.

INTRODUCTION

Parallel MRI is one of the most fascinating aspects of modern MRI. It makes use of the very basic insight that an array of multiple radiofrequency (RF) coils performs better than a single RF coil. Although this idea is almost as old as MRI itself, the real breakthrough with this idea happened in the last decade. It started with the introduction of coil arrays for improving RF acquisition (what is called *parallel imaging*). An analogous transition can now be observed for RF transmission (*parallel transmission*). In accord with this twofold development, the presentation here is split into a parallel imaging and a parallel transmission part. For both approaches, the basic principles, the main advantages, and central application areas are outlined. Note that, although both approaches are based on the same idea of multiplying RF coils, the consequences differ significantly. These differences are sketched separately, at the end of the article.

PARALLEL IMAGING

Parallel imaging is based on the idea that the spatially varying sensitivities of individual coil elements forming a receive coil array can be used to instantaneously encode spatial information during signal reception. This simultaneous signal encoding allows for the reduction of the number of necessary phase-encoding steps conventionally required for magnetic resonance imaging and thus the acceleration of scanning or the increase of spatial resolution, keeping the total scan time constant.

The development of parallel imaging began with the introduction of the phased array coil concept[1] as a suitable hardware platform to increase the signal-to-noise ratio. Multiple independent and decoupled reception coils each connected to an individual receiver allowed a local signal reception, minimizing the noise, dominated by the object itself, to the sensitive volume of the coil. Different algorithms have been elaborated to combine the individual coil data and to compensate for the residual reception inhomogeneities.[1] Some of these approaches already partly anticipated recent developments in parallel imaging and have, therefore, something in common with algorithms used for approaches to accelerate scanning.

In contrast to some early ideas,[2,3] which tried to overcome conventional phase encoding completely, recent approaches to accelerated parallel imaging perform sensitivity and phase encoding simultaneously, to reduce the number of necessary phase-encoding steps.[4–8]

Thus, all accelerated parallel imaging approaches perform subsampling in *k*-space, which in general makes image reconstruction a little more complicated than just using the Fourier transform. A number of different techniques have been introduced, which can coarsely be subdi-

Address correspondence and reprint requests to: Ulrich Katscher, Philips Research Europe-Hamburg, Roentgenstrasse 24-26, 22335 Hamburg, Germany. E-mail: Ulrich.Katscher@philips.com.

vided according to the two domains (*k*-space/image-space) in which processing is mainly performed. SMASH[6,9] (which stands for simultaneous acquisition of spatial harmonics) was proposed as an approach to perform parallel imaging in *k*-space. The same holds for GRAPPA (for *generalized autocalibrating partially parallel acquisition*),[8] a further refinement that incorporates the idea of autocalibration. In contrast to these, the processing in SENSE[7] (for *sensitivity encoding*) is performed in the spatial domain. PILS[10] (for *parallel imaging with localized sensitivities*) has been introduced as another simple and robust approach that also works in the spatial domain.

The strict distinction between *k*-space and image domain is rather impractical in the current world, however. Numerous generalizations and refinements have been elaborated. The SMASH reconstruction has been generalized to provide tailored harmonic fits,[11] and a generalized matrix formulation[12] has been elaborated. SENSE has been applied to arbitrary *k*-space trajectories,[13] including nonuniform sampling in the phase-encoding direction,[14] making it difficult to solve the problem solely in the spatial domain. Furthermore, it is possible to include the time axis into the concept of parallel imaging, to take advantage of the spatiotemporal correlation in the acquired MRI data.[15,16]

Parallel imaging started out by using RF coil arrays consisting only of a few elements.[6,7] Since then, however, arrays of 32 independent elements are becoming standard for clinical systems.[17,18] MRI systems with up to 128 RF channels are expected to become available in the near future,[19–21] requiring new developments of the involved hardware as well as of image reconstruction. Continuing in this direction, it might be that the original dream of parallel imaging will come true at last: to overcome the phase encoding completely.

The basic problem

A detailed and general formulation of (accelerated) parallel imaging and a corresponding performance analysis is given by Pruessmann et al.[7] In all recently used accelerated parallel imaging schemes, phase encoding is performed, and the signal in the individual channels is encoded simultaneously by means of the corresponding coil sensitivities. The signal $m_j(\mathbf{k})$ received by a certain reception coil j can thus be given as

$$m_j(\mathbf{k}) = \int_R \rho(\mathbf{r})\, s_j(\mathbf{r}) \exp(-i\mathbf{k}\mathbf{r})\, d\boldsymbol{r}, \qquad (1)$$

where ρ denotes the signal density in the spatial domain, $s_j(\mathbf{r})$ the corresponding spatial coil sensitivity, and $\mathbf{k}$ the *k*-space coordinate. The exponential term stands for the conventional Fourier encoding, and the coil sensitivity $s_j(\mathbf{r})$ represents the sensitivity encoding. In a discrete version, the problem can be formulated using the corresponding encoding matrix E, which can be given as[7]

$$E_{(j,\kappa)|\rho} = \exp(i\mathbf{k}_\kappa \mathbf{r}_\rho) s_j(\mathbf{r}_\rho), \qquad (2)$$

where the index j denotes the coil with the corresponding spatial sensitivity $s_j(\mathbf{r})$, $\mathbf{k}_\kappa$ the *k*-space coordinate given at the κ-th sampling position, and $\mathbf{r}_\rho$ indicates the spatial coordinate at the ρ-th voxel. Thus, the measured data m can be given as

$$m = \mathrm{E}f \qquad (3)$$

where f denotes the spatial magnetic resonance signal distribution (i.e., the image to be obtained). Noise is superimposed on the signal m and cannot be affected by the encoding process.

The image reconstruction or the solution of the inverse problem of Eq. (3), which is optimal in the least square sense, can be given as[7]

$$f = \left(\mathrm{E}^{\mathrm{H}}\Psi^{-1}\mathrm{E}\right)^{-1}\mathrm{E}^{\mathrm{H}}\Psi^{-1}m, \qquad (4)$$

where the bracketed term has the form of a pseudoinverse; Ψ denotes the noise covariance, which describes the stochastic correlation of the noise in the individual coil signals, and the superscript H indicates the complex conjugate transpose.

Equation (4) is the general formulation of the solution of the inverse problem, which can be rather demanding for arbitrary *k*-space trajectories[13,14] and will be discussed in a later section.

SENSE

For sampling schemes with uniformly subsampled *k*-space, the complexity given in Eq. (2) can be reduced considerably. This is the case of Cartesian schemes, in which the sampling density in phase-encoding direction can be reduced according to the chosen reduction factor *R*. This means that the intersampling line spacing is increased, which corresponds to a sampling of a data set in a field of view (FoV) reduced by the factor *R*. However, *k*-space has to be covered up to the same maximum *k*-values, which are reached in a nonaccelerated scan, to fulfill the sampling theorem for the desired voxel resolution. In the case of uniform subsampling, Eq. (2) and Eq. (4) can be simplified F1)(FIG. 2). The sensitivity encoding can be decoupled from the phase encoding, and an intermediate set of images can be obtained for each coil via Fourier transform based on the reduced *k*-space data sets:

$$S_{(j,\rho)} = s_j(\mathbf{r}_\rho). \qquad (5)$$

Here, $\mathbf{r}_\rho$ again stands for the spatial coordinate of the ρ-th voxel, which folds into the reduced FoV data set of the j-th coil according to the point-spread function (PSF) of the subsampling scheme. Now, the inverse problem has to be solved. Thus, for each set of voxels in the full FoV,

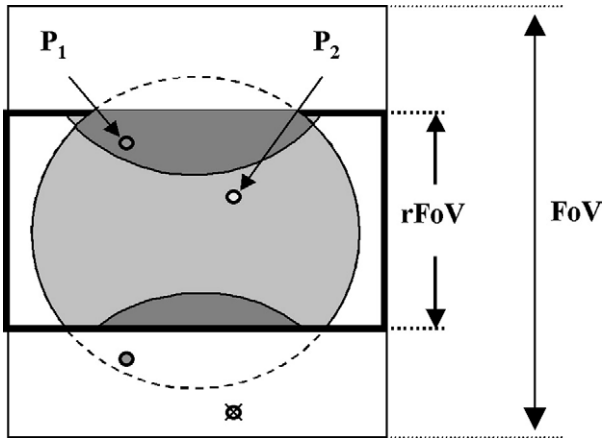

FIG. 1. Foldover in the subsampled (reduced) FoV for a reduction factor $R = 2$ results in aliasing artifacts. Based on the coil sensitivity information, these will be unfolded in SENSE. These images show clearly the corresponding foldover artifacts described by the point-spread function (PSF) of the uniform subsampling scheme. In pixel P_1, a pixel from outside the rFoV is superposed, which is not the case for pixel P_2. Due to Fourier transform, the impact of phase encoding (see Eq. [2]) has already been decoded, but the sensitivity encoding is still left. The reconstruction problem has thus been transferred into the spatial domain, and its complexity has been reduced considerably. The effective encoding matrix given in Eq. (2) now modifies to the coil sensitivity matrix S. *Abbreviations:* FoV, field of view; rFoV, reduced field of view.

the contributions from folded pixels in the individual subsampled coil images have to be extracted. As a result of this simplification, Eq. (4) can be given as

$$\mathrm{f}' = \left(\mathrm{S}^{\mathrm{H}}\Psi^{-1}\mathrm{S}\right)^{-1}\mathrm{S}^{\mathrm{H}}\Psi^{-1}\mathrm{m}'. \qquad (6)$$

The vector f' in Eq. (4) contains the separated voxel signals, whereas the vector m' is built out of the folding voxel signals in the reduced FoV images of the individual coils. Once f' is obtained, the signals can be filled in the full FoV. This procedure has to be repeated for each voxel in the reduced FoV to obtain a solution for the full FoV. The size of the unfold problem can vary from voxel to voxel, which means that the number of voxels superimposed can change. This is especially the case, if noninteger reduction factors are used during data acquisition. As a consequence, the degree of overdetermination can vary, which may have some impact on the stability of the inversion process given in Eq. (6). If there is some a priori knowledge available, which allows excluding those voxels that cannot carry any signal, stability can be further improved.[22]

The described concept can be extended to two or even three spatial dimensions.[22,23] In particular for three-dimensional scans, the *k*-space might be subsampled in the two phase-encoded directions, which can increase the reconstruction stability for a given total reduction factor considerably.

Optimal coil signal combination

The SENSE reconstruction shows very notable similarities to the optimal coil signal combination proposed by Roemer et al.[1] In their article, parallel imaging without scan acceleration is discussed, aiming at signal-to-noise ratio maximization due to optimal coil signal combination. This is achieved by weighting the coil signals prior to addition with their local sensitivity to either suppress noise contributions from regions far away from their sensitive volumes and to phase the individual coil signal contributions per voxel properly to avoid signal cancellation during the final superposition. Thus, we note, Eq. (6) also gives the solution to the problem of optimal coil combination,[1] obviously, if a reduction factor $R = 1$ is considered. This similarity underscores an additional important point inherent to the SENSE approach: it combines all data in the optimal signal-to-noise ratio sense.

The weighting of the individual coil signals by their corresponding sensitivity can be further developed to give a simple parallel imaging reconstruction in the spatial domain, even if subsampling is performed. One example is the PILS approach.[10] In this approach, the spatial base of the individual reception coils is restricted to avoid foldover in the final image. This can be understood as a simple spatial filtering procedure. With the knowledge of the spatial position and the sensitive area of each individual coil, which can be easily derived from their sensitivity $s(\mathbf{r})$, the corresponding signal contributions in the reduced FoV can be adequately chopped to suppress foldover. Subsequently, these subregions can be concatenated in the full FoV to form the final image.

From SMASH to GRAPPA

The reconstruction of undersampled data can also be performed in the *k*-space domain. If the mathematical operations (multiplication and addition) given in Eq. (4) were to be performed in *k*-space, the result would be a convolution with a truncated kernel, which is generated from a set of harmonic fits to the coil sensitivities.[24] This convolution would smear out the measured data in *k*-

$$\Sigma_j\, n_j(l)\, s_j(y) = \exp(i\, l\, \Delta k_y\, y)$$

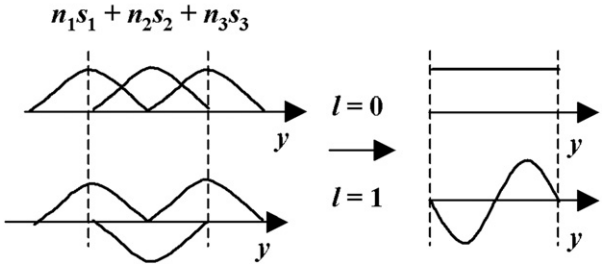

FIG. 2. Schematic representation of the fitting procedure in SMASH (Eq. [8]) to obtain spatial harmonics as a superposition of the coil sensitivities s_j.

space, which would allow predicting the values for the missing lines in *k*-space.

Thus, according to the encoding problem given in Eq. (2), the SMASH approach tries to estimate the missing data in *k*-space, but in a single, composite *k*-space matrix. The missing lines are obtained as a linear combination of measured coil data. An appropriate fitting process determines the corresponding weights n_j, which transform the signal of a single measured line (m_j) for each of the coils with the sensitivity s_j into a shifted line in the composite *k*-space matrix (m′):

$$m'(k_y - l\,\Delta k_y) = \sum_j n_j(l)\, m_j(k_y). \qquad (7)$$

The necessary coil-specific weighting coefficients $n_j(l)$ are calculated according to Eq. (8) by a fit to the l-th harmonic (FIG. 2), and the term Δk_y denotes the desired *k*-space increment:

$$\sum_j n_j(l) s_j(y) = \exp(i\, l\, \Delta k_y\, y). \qquad (8)$$

Thus, the SMASH reconstruction could be viewed as an approach that tries to mimic conventional phase encoding by forming spatial encoding functions of the Fourier harmonic type by an appropriate superposition of the data sampled with the coils of different sensitivities. The early SMASH implementations used coil sensitivity maps measured in the spatial domain to derive the corresponding reconstruction parameters. Sometimes, a substantial mismatch between the actual fit and the desired spatial harmonics was found, which could be overcome by more sophisticated procedures[11] and dedicated phase corrections.

To become independent from the extra coil sensitivity information, which could be sensitive to a number of adverse effects like noise, patient motion, off-resonance or aliasing, autocalibrated approaches have been developed (AUTO-SMASH, VD-AUTOSMASH, GRAPPA).[8,26,27] In these approaches, a number of central *k*-space lines are additionally acquired, containing what is called the *autocalibration signal* (ACS). Thus, *k*-space is sampled with a variable density. The necessary reconstruction parameters are determined again in *k*-space, but now by fitting the signal of several measured lines grouped as blocks in *k*-space to the signal of the ACS lines for each coil independently. The weights $n_j(l)$ are determined by fitting a reduced dataset to an ACS line:

$$\sum_j m_j^{\mathrm{ACS}}(k_y - l\,\Delta k_y) = \sum_j n_j(l)\, m_j(k_y). \qquad (9)$$

This was further refined in the variable density AUTO-SMASH[27] approach, which performs this fitting procedure for a number of lines (FIG. 3).

The GRAPPA technique represents a more generalized implementation of these AUTO-SMASH approaches.[8] In contrast to SMASH, which estimates data in a composite

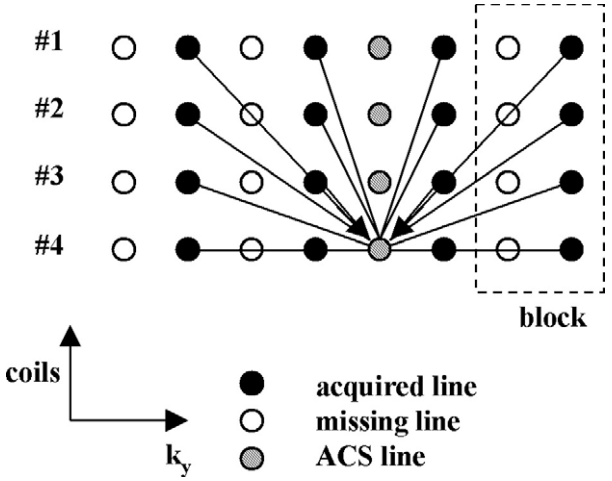

FIG. 3. Scheme of the GRAPPA approach. Multiple lines acquired for the different coils are fitted to the autocalibration signal (ACS) data. Here, four lines are employed to fit a single ACS line in coil 4. The dotted line area indicates a block used in the GRAPPA approach.

k-space matrix, GRAPPA uses data from multiple lines to fit a line in each single coil *k*-space. Based on the weighting coefficients $n_j(b, l)$, the other missing lines for this particular coil can be estimated (the index b indicates the chosen block size[8] in *k*-space):

$$m_j(k_y - l\,\Delta k_y) = \sum_j \sum_b n_j(b, l) m_j(k_y - l\,\Delta k_y). \qquad (10)$$

This coil-dependent procedure is performed for all coils to fill the missing lines in their *k*-space data prior to Fourier transform. The resulting images can be combined using a simple sum of squares or more optimized versions as well.[1]

These autocalibrating approaches allow the acquisition of the reference data at the same time as the reduced *k*-space data are measured. Thus, the same state of the object is reflected, and the ACS lines can be incorporated into the reconstruction to increase the signal-to-noise ratio. This advantage has to be paid for, however, with a small loss in the effective acceleration rate. If this is a problem, ACS line acquisition can be decoupled from the actual scan.

Nonuniform sampling

In the preceding sections, we have looked at the Cartesian uniform subsampling schemes. These allow separating the spatial Fourier encoding from the sensitivity encoding. According to the spatially sharply defined PSF, the folding signal contributions from the different spatial locations can be separated. This becomes more difficult in the case of nonuniform *k*-space sampling schemes.[13] The corresponding PSFs couple numerous spatial locations, making a solution in the spatial domain very difficult. Consequently, the full inverse problem given in Eq. (2) has to be addressed.[13,14] This turns out

to be very demanding, however, if it is done directly by means of linear algebra. The solution would require the inversion of huge matrices, for example a $N^2 \times N^2$ matrix for an $N \times N$ image, which might be challenging for usual image sizes. However, iterative approaches have been proposed to handle problems of this complexity at a sufficient convergence.[13]

In addition, *k*-space based approaches such as SMASH and GRAPPA have been adapted to nonuniform sampling schemes as interesting alternatives.[28,29] These alternatives benefit from the fact that most non-Cartesian sampling schemes sample the center of *k*-space denser, which supports autocalibration easily.

Reconstruction stability and data consistency

All parallel imaging–based image reconstruction approaches involve linear algebra expressed by a matrix inversion. If the corresponding problem is ill-posed, the error propagation can result in a serious problem. During the inversion process, noise present in the input data can be amplified in the final images. In this context, Pruessmann et al.[7] developed the concept of the geometry factor, which is applicable to uniform Cartesian subsampling schemes. The geometry factor quantifies this effect in the spatial domain.

In most cases, the inverse problem is overdetermined, which means there are more equations than variables to be determined. To increase the stability of the inversion process, a number of different numerical tricks can be used—regularization techniques, in particular. Regularization allows compensating for small errors in sensitivities and ill conditioning that can amplify noise during the inversion process. Regularization can be performed using a fixed threshold parameter, by incorporating a priori knowledge, or by using a first-guess of the image to be reconstructed,[30] reducing all kinds of potential divergences. On the other hand, singular value decomposition can be applied to remove the smallest eigenvalues prior to inversion.[25,31–34] Regularization can further be understood as the integration of constraints into the reconstruction process. It has to be applied very carefully, because it can affect the image information content.

Recently, there is a trend toward MRI systems equipped with 32 or more independent receive channels.[17–21] Systems equipped with appropriate reception coils allow for high scan acceleration factors. However, reduction factors cannot be increased linearly with the number of receive coil elements, because of MRI intrinsic signal-to-noise ratio limitations.[35] Consequently, the parallel imaging reconstruction problem becomes more overdetermined, creating a high level of data redundancy.

Usually, this redundancy is exclusively used for signal-to-noise ratio optimization in the reconstructed image.[36] The extra data do contain additional information, however, and can help to increase the robustness and reliability of the reconstruction with respect to any nonideal condition during the scan.[37–43] The additional information allows a check on any consistency of the image reconstruction to identify image artifacts.[39,41] Such artifacts could result from all kind of inconsistencies in the acquired data—in particular from patient motion, but also from steady-state problems, sampling theorem violations, coil sensitivity errors, and the like. These artifacts can be identified, marked, and corrected by analyzing and using the data redundancy in parallel imaging, which could make scanning even more robust in the future.

Applications

Neurological applications, which represent a major area of application, benefit greatly from parallel imaging. This imaging technology improves either or both temporal and spatial resolution of functional MRI,[44–48] offering more detailed and sophisticated *in vivo* studies. Furthermore, susceptibility-induced image artifacts can be reduced considerably by shortening the read-out length of the usually applied echo-planar schemes, which is advantageous in areas near the base of the skull. In addition, parallel imaging can considerably accelerate and improve diffusion-weighted imaging,[49,50] which finds important applications in the diagnostics of stroke[51,52] and in fiber tracking,[53–55] by keeping total measuring time within acceptable limits. Finally, by shortening the total measuring times, parallel imaging helps to further pave the way for spectroscopic imaging[56–59] in a clinical setting.

Cardiovascular diagnostics represent another very important application area of parallel imaging. Here, it helps to achieve the necessary temporal and spatial resolution required to follow the fast cardiac motion.[60–62] Coronary magnetic resonance angiography benefits much from the potential of shortening total scanning times,[63,64] which pays back in image quality due to the increased patient comfort. Contrast-enhanced angiography gains greatly if performed using parallel imaging.[65–67] Increasing the temporal resolution improves the diagnostic value and avoids bolus dilution of the applied contrast media, which considerably improves the contrast-to-noise ratio.[65] Parallel imaging furthermore enables single breath-hold acquisitions in the abdominal region, helping to reduce respiratory motion artifacts.[68,69]

Figure 4 shows an example of a ninefold accelerated abdominal image, together with selected individual, folded images.

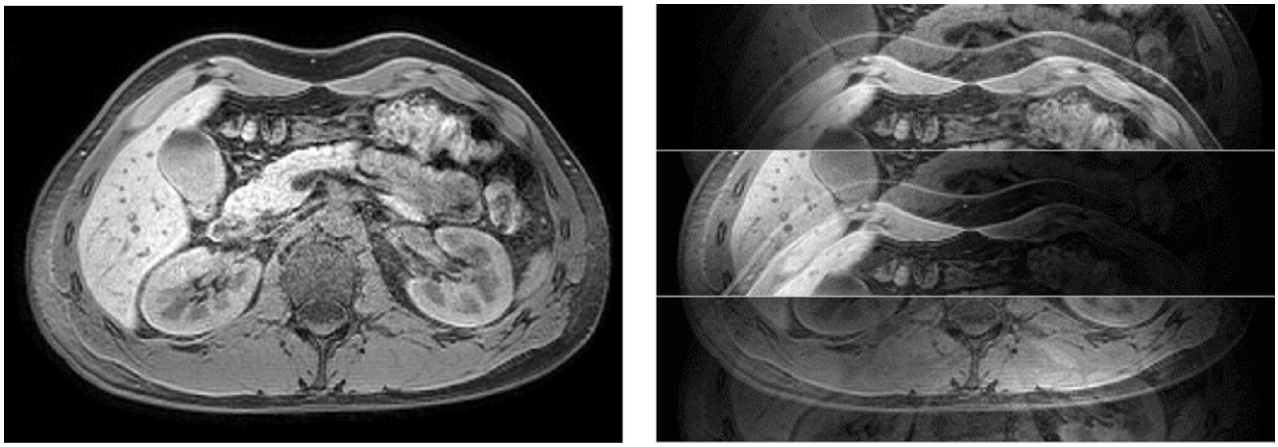

FIG. 4. In vivo SENSE example acquired with a T1-weighted gradient echo sequence and a fat-suppression radiofrequency (RF) prepulse. Left: Reconstructed image using 32 receive coils and a total reduction factor of $R = 9$ ($R = 3$ through-plane and $R = 3$ in-plane anterior–posterior). The noise enhancement in the central region is due to the geometry factor reflecting the conditioning of the reconstruction problem. Right: Partially unfolded images of three selected coils of the array. For demonstration purposes, images are unfolded only in through-plane direction to visualize the in-plane folding. In practice, combined unfolding in both directions is performed in a single step.

PARALLEL TRANSMISSION

Equivalent to parallel imaging, multiple transmit coils have been proposed to perform parallel transmission. The idea was triggered by the introduction of human high-field MRI systems, which show B_1 uniformity problems caused by wave-propagation effects.[70–72] Thus, multiport excitation for birdcage-type coils was proposed as a measure to improve the RF homogeneity in the excited volume.[73,74] The underlying hardware can be considered as a multielement transmit coil array, which allows changing the phase and amplitude of the otherwise identical RF waveforms for the individual ports. Meanwhile, the basic feasibility of this RF shimming concept has been shown.[75–78]

Triggered by these hardware developments and based on the analogy between RF pulse design and MRI,[79,80] the principles of parallel imaging have also been applied to RF transmission.[81,82] Thus, RF pulses were proposed that are controlled by completely different time-courses in the individual transmit channels. This degree of freedom offers the possibility to improve spatially selective multidimensional RF pulses[83–90] (e.g., by shortening the pulse duration, enhancing their spatial definition, or reducing their required RF power).

The basic problem

In parallel imaging, *k*-space is typically undersampled, and data acquisition is performed with a number of individual receive coils. The resulting image artifact is avoided by taking the coil sensitivity information during image reconstruction into account. Consequently, the central question in parallel imaging might be formulated thus: given a couple of measured, particularly undersampled data sets from individual coils, how does one obtain a single, complete image? As we have already noted, this question has been answered so far by Roemer et al.,[1] Sodickson and Manning,[6] and Pruessmann et al.[7]

Similarly, in parallel transmission, each individual transmit coil could excite a specific magnetization pattern that may show artifacts, in particular caused by subsampling of the excitation *k*-space or B_1 nonuniformities. However, their parallel superposition should result in the desired artifact-free magnetization pattern. Thus, the question is: which spatial patterns $P_i(\mathbf{r})$, that might show undersampling effects, have to be excited by each of the N transmit coils, each exhibiting a characteristic sensitivity profile $S_i(\mathbf{r})$, to obtain the desired excitation pattern $P_{\text{des}}(\mathbf{r})$? This constraint leads to Eq. (11), which turns out to be the central equation of parallel transmission:

$$P_{\text{des}}(\mathbf{r}) = \sum_{i=1}^{N} S_i(\mathbf{r}) P_i(\mathbf{r}). \qquad (11)$$

Here, $P_{\text{des}}(\mathbf{r})$ is defined within the field of excitation (FoX), given on *m* spatial positions in a one-, two-, or three-dimensional array. Equation (11) is linear and states that the superposition of all the individual pulse profiles $P_i(\mathbf{r})$, weighted by the corresponding (complex) coil sensitivity profiles, should yield the desired excitation pattern. It is assumed, that the $S_i(\mathbf{r})$ are known by means of B_1 mapping techniques.[91–93] If the transmit coils can be used in the receive mode, methods known from parallel imaging can be employed,[6,7] assuming the principle of reciprocity holds. To derive the unknown RF waveforms $B_{1i}(t)$ for the *N* individual transmit coil elements from Eq. (11), the following steps have to be performed.

Equation (11) has to be transformed into the Fourier domain (the excitation *k*-space). Thus, instead of the

unknown $P_i(\mathbf{r})$ given in Eq. (11), now the equation contains the unknown $p_i(\mathbf{k})$

$$P_{\text{des}}(\mathbf{k}) = \sum_{i=1}^{N} s_i(\mathbf{k}) \otimes p_i(\mathbf{k}). \tag{12}$$

This step is performed because the B_1 waveform that excites a desired magnetization pattern is just its Fourier transform sampled along the chosen excitation *k*-space trajectory multiplied by some trajectory-dependent weighting coefficients. This is according to the RF pulse design concept of Pauly et al.,[79] based on the low tip angle approximation, which might hold for even higher flip angles for special *k*-space trajectories.[94]

In a slightly different writing of Eq. (12), as given by Grissom et al.,[95] only the $P_i(\mathbf{r})$ in Eq. (11) are transformed to the Fourier domain, introducing the Fourier encoding matrix $A \sim \exp(i\mathbf{rk})$:

$$P_{\text{des}}(\mathbf{r}) = \sum_{i=1}^{N} S_i(\mathbf{r}) A(\mathbf{r}, \mathbf{k}) p_i(\mathbf{k}). \tag{13}$$

This specific approach eases the restriction of the excitation pattern $P_{\text{des}}(\mathbf{r})$ to a finite area inside the FoX. To separate the wanted $p_i(\mathbf{k})$, Eq. (12) has to be inverted, which is nontrivial in case of an arbitrary *k*-space trajectory. To facilitate inversion,[81] the *k*-space transformed coil sensitivities $s_i(\mathbf{k})$ are grouped into a single, invertible sensitivity matrix s_{full}. Additionally, a corresponding single vector p_{full} is formed from the individual $p_i(\mathbf{k})$

$$p_{\text{des}}(\mathbf{k}) = s_{\text{full}}(\mathbf{k}) p_{\text{full}}(\mathbf{k}). \tag{14}$$

This reformulated equation can then be solved using the pseudoinverse (regularized with the free parameter λ), which is the optimal solution in the least square sense:

$$p_{\text{full}} = s_{\text{full}}^{H} \left(s_{\text{full}} s_{\text{full}}^{H} + \lambda \right)^{-1} p_{\text{des}}. \tag{15}$$

The free regularization parameter λ stabilizes the reconstruction in the case of an ill-posed sensitivity matrix. It pushes the reconstruction to favor solutions p_{full} with a minimum norm. The individual excitation patterns $p_i(\mathbf{k})$ can be extracted from p_{full}, which represents the general solution without any constraints. The separation of the $p_i(\mathbf{k})$ starting from Eq. (13) instead of Eq. (12) can be performed in an analog way.

Now, the special case is considered of a Cartesian, echo-planar-like *k*-space trajectory, which is uniformly undersampled in one dimension. Consequently, only a limited number of voxels account for folding in the spatial domain, which is described by the corresponding PSF of the sampling scheme. As known from parallel imaging, this special case can be solved in the spatial domain[7] and leads to a small size of the sensitivity matrix being inverted. This approach was chosen by Zhu,[82] with the solution for the $p_i(\mathbf{k})$ written as an integral over the FoX:

$$p_i(\mathbf{k}) = \int_{\text{FoX}} h_i(\mathbf{r}) P_{\text{des}}(\mathbf{r}) e^{-i2\pi \mathbf{kr}} d\mathbf{r}. \tag{16}$$

In this equation, the h_i are derived from the inversion of a sensitivity matrix $C(S_1(\mathbf{r}), S_2(\mathbf{r}), \ldots, S_N(\mathbf{r}))$.[82] The inversion of this sensitivity matrix C is the central step of the approach and might be compared with the inversion of the matrix s_{full} (Eq. [14]). Both matrices s_{full} and C depend solely on the spatial sensitivity distributions S_i, but differ in their detailed definitions.[81,82] Once the $p_i(\mathbf{k})$ are calculated via Eq. (15) or (16), the mapping between $\mathbf{k}$ and t has to be performed according to the chosen *k*-space trajectory. This yields the actual B_1 waveforms applied in the time domain. The weighting function $W(t)$ reflects the *k*-space sampling density, which is constant for Cartesian trajectories and takes the *k*-space velocity (i.e., the actual gradient) into account.[79] The wanted waveforms can be calculated for each individual coil via

$$B_{1i}(t) = W(t) p_i(\mathbf{k}(t)). \tag{17}$$

The resulting degree of freedom introduced by the use of multiple transmit coils can be exploited in several directions. A major application is given by the reduction of the pulse duration by a factor *R*, corresponding to the reduction of acquisition time in parallel imaging. Instead of reducing the pulse duration, the spatial definition of the excitation pattern can be increased without changing the pulse duration. Furthermore, system imperfections such as B_0 inhomogeneities, *k*-space trajectory imperfections, concomitant gradients effects, and the like can be compensated for.[80,96]

Another application of multiple transmit coils is to reduce the required RF power, and thus, the specific energy absorption rate (SAR).[82,97–100] The intrinsic freedom in solving Eq. (11) can be used to favor those solutions that exhibit the lowest RF power. This can be realized, for example, by regularization (Eq. [15]), wherein the overall pulse power is added to the error function to be minimized.[99] In a more sophisticated model, not only the RF power but also the SAR can be taken into account by calculating the corresponding electric fields in the patient.[82]

As we have mentioned, a different form of parallel transmission is performed for the purpose of RF shimming, which is desirable especially for high-field applications. Here, the amplitudes A_i and phases φ_i of the otherwise identical B_1 waveforms are adjusted for the different transmit array elements to yield optimal spatial excitation homogeneity.[73–75] This is also described by Eq. (11). The optimum A_i and φ_i can be derived if the individual excitation patterns $P_i(\mathbf{r})$ are replaced by constant weighting factors $F_i = A_i \exp(i\varphi_i)$, which are spa-

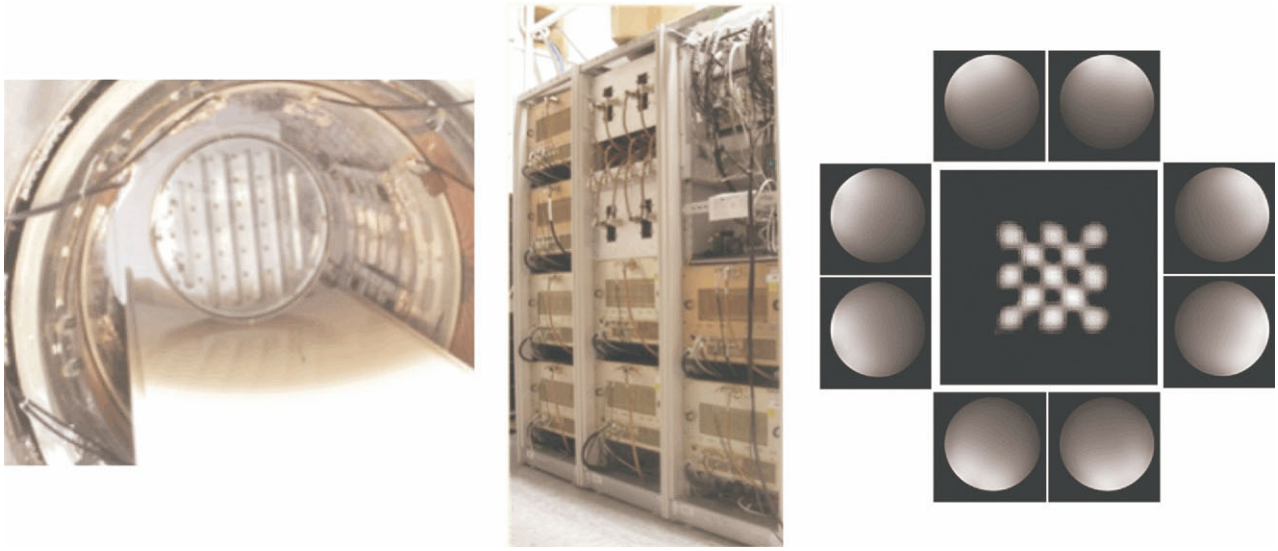

FIG. 5. Example of a whole-body MRI system equipped with eight independent transmit–receive channels.[107] Left: Transmit–receive RF coil with eight cylindrically arranged transverse electromagnetic elements,[105] and quality phantom. Center: Corresponding cabinets showing eight RF amplifiers, two circulator boxes (central cabinet) and the fully integrated spectrometer (right cabinet). Right: Transmit sensitivities of the eight transmit elements and checkerboard pattern excited via parallel transmission, using a spiral *k*-space trajectory and a reduction factor $R = 2$.

tially invariant. In this case, Eq. (11) can be solved for the F_i via a matrix inversion in the spatial domain choosing a constant $P_{des}(\mathbf{r})$. Obviously, a nonconstant $P_{des}(\mathbf{r})$ might be chosen in this framework as well. In contrast to this basic RF shimming, a (parallel-transmitted) spatially selective RF pulse can be also used to compensate for B1 inhomogeneities, leading to a tailored RF shimming.[101]

Experimental proof

The theoretical development of parallel transmission preceded the corresponding experimental abilities by several years. Thus, the first experimental proofs mimicked parallel transmission in sequential experiments using different transmit coils and making use of the linearity of the problem (see Eq. [11]) by superimposing their results after signal acquisition.[81,82] With the development of multielement–transmit coils,[102–105] parallel transmission has been used to perform basic RF shimming[75–78] by varying amplitudes and phases for the individual channels.

A full verification of the entire concept was accomplished by the introduction of prototype MRI systems,[78,106–108] which allowed driving the RF waveforms individually for each channel. Thus, spatially selective 2D RF pulses, using different *k*-space trajectories, have been considerably accelerated. Figure 5 shows the example of a whole-body MRI system equipped with eight independent transmit–receive channels.[105,107]

Signal-to-noise ratio and SAR

Noise that might degrade the performance of parallel transmission might originate from the digital-to-analog converting process and RF amplifier imperfections. This system noise affects the individual pulse profiles $P_i(\mathbf{r})$, and thus influences the final result in a linear way as a superposition in the spatial domain (see Eq. [11]). Errors in the coil sensitivity profiles caused by noise or measurement imperfections also influence the final result linearly via Eq. (11). It is important to note that the system noise does not interact with the central matrix inversion (see, for example, Eq. [15]). This is a crucial difference with respect to parallel imaging, in which the system noise generated in the receive chain is enhanced, if the matrix inversion is ill conditioned.[7] In parallel imaging, the inverted matrix is multiplied with the measured data bearing noise. In parallel transmission, the inverted matrix is multiplied with the desired excitation pattern, which is free of noise (FIG. 6).

If the inverse problem of parallel transmission is ill-posed, the superposition of Eq. (11) does not lead to a complete cancellation of the subsampling artifacts, and

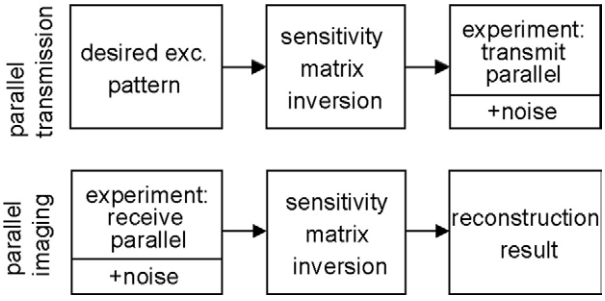

FIG. 6. Schematic comparison of parallel transmission and parallel imaging. Experimental noise comes into play after (for parallel transmission) and before (for parallel imaging) the inversion of the sensitivity matrix, which leads to a larger robustness of parallel transmission than parallel imaging.

noise-like aliasing structures appear in the final result. The problem becomes ill-posed if the spatial frequency components of the actual coil sensitivity profiles cannot compensate for the missing parts of a reduced *k*-space trajectory. Thus, a proper interplay between the coil sensitivity profiles and the involved trajectories has to be found. Simulations have shown, however, that RF pulse performance is in general rather robust against variations of the transmit coil array configuration and becomes critical only for very artificial cases.[109]

In that respect, the concept of the geometry factor as deduced for parallel imaging[7] cannot be adapted directly to parallel transmission. For parallel transmission, corresponding concepts describing the occurring SAR can be derived.[110] If the sensitivity matrix s_{full} to be inverted becomes ill-posed, the norm of the resulting vector p_{full}, containing the RF waveforms, may increase (see Eq. [14]). This increase would lead to an increase of the required RF power and the SAR, respectively. Thus, SAR could serve as an important coil design criterion, but it has been found that the RF pulse performance again proves to be fairly stable.[109,111]

The question of an ill-posed inverse problem seems to play only a minor role in parallel transmission. This gives rise to a much larger freedom in designing coil arrays for parallel transmission than for parallel imaging. Nevertheless, a thorough investigation of SAR to ensure patient safety is required.[112]

Applications

Currently, only a very limited number of MRI prototype systems worldwide are capable of parallel transmission. With the increasing availability of corresponding systems, it is expected that more and more applications will be developed and tested. Today, the following potential applications of parallel transmission can be foreseen:

- compensation of patient induced RF inhomogeneities,[89,90] particularly at main fields of 3 T and 7 T,
- volume-selective excitation[79,83,84] for zoom imaging, investigation of perfusion and diffusion, or localized spectroscopy,
- curved slice imaging,[85] and
- navigators applied for motion sensing.[86]

Furthermore, parallel transmission might ease the application of 3D RF pulses,[87,88] which are limited by the finite lifetime of the transverse magnetization and the main field homogeneity.

PARALLEL IMAGING AND PARALLEL TRANSMISSION: A COMPARISON

Parallel transmission is not simply the reciprocal of parallel imaging. Both approaches are a combination of a forward and an inverse matrix problem. Neither the front end of the MRI system (i.e., the coil array) nor the spin system of the patient's body is capable of inverting a matrix. The MRI scanner can, however, superimpose all kinds of magnetic fields to act on the magnetization, which is equivalent to solving a forward problem. The inverse problem has to be solved on the host computer (i.e., the back end of the MRI system). The data flow from the back end to the front end for parallel transmission, and vice versa for parallel imaging. Note, however, that when the inverse problem is to be solved it cannot be shifted from the back end to the front end. The inverse problem must be solved on the back end of the MRI system, irrespective of the direction of the data flow. This might explain why parallel transmission cannot be derived by simply inverting the parallel imaging algorithm, or vice versa.

Parallel imaging is based on the acquisition *k*-space, parallel transmission on the excitation *k*-space. Thus, the main goal of parallel imaging is the shortening of the acquisition time. The main goal of parallel transmission is the shortening of the pulse duration of spatially selective RF pulses. Shortening RF pulses reduces the total acquisition time only marginally; however, local excitation via (shortened) spatially selective pulses can be used to reduce the necessary FoV, which again leads to a reduction of the total acquisition time.

Another important difference is described by the geometry factor (see the sections "Reconstruction stability and data consistency" and "Signal-to-noise ratio and SAR"). For parallel imaging, a suboptimal geometry of the coil array leads to a nonlinear enhancement of the noise in the reconstructed image.[7] For parallel transmission, a suboptimal geometry of the coil array leads to a nonlinear enhancement of the SAR.[110] Both aspects are of crucial importance, and numerous studies have been performed to minimize these effects; however, an array geometry suitable for parallel imaging is also suitable for parallel transmission. Thus, the use of coil arrays capable for both (i.e., RF transmit and receive) is in general possible, which eases coil array design.

Parallel imaging and parallel transmission can themselves be performed in parallel—that is, both approaches can be applied during a MRI sequence without any interference. As noted, the same coil array can be used for both approaches. The multiplication of the whole receive and transmit channel differs tremendously, however, requiring an almost complete redesign of the spectrometer and the software of the MRI system.

Acknowledgments: The authors cordially thank Ingmar Graesslin, Peter Vernickel, and Richard Winkelmann for their contributions.

REFERENCES

1. Roemer PB, Edelstein WA, Hayes CE, Souza SP, Mueller OM. The NMR phased array. Magn Reson Med 1990;16:192–225.
2. Carlson JW. An algorithm for NMR imaging reconstruction based on multiple RF receiver coils. J Magn Reson 1987;74:376–380.
3. Hutchinson M, Raff U. Fast MRI data acquisition using multiple detectors. Magn Reson Med 1988;6:87–91.
4. Kelton JR, Magin RL, Wright SM. An algorithm for rapid image acquisition using multiple receiver coils. Proc Soc Magn Reson Med 1989;1172.
5. Ra JB, Rim CY. Fast imaging using subencoding data sets from multiple detectors. Magn Reson Med 1993;30:142–145.
6. Sodickson DK, Manning WJ. Simultaneous acquisition of spatial harmonics (SMASH): fast imaging with radiofrequency coil arrays. Magn Reson Med 1997;38:591–603.
7. Pruessmann KP, Weiger M, Scheidegger MB, Boesiger P. SENSE: sensitivity encoding for fast MRI. Magn Reson Med 1999;42:952–962.
8. Griswold MA, Jakob PM, Heidemann RM, et al. Generalized autocalibrating partially parallel acquisitions (GRAPPA). Magn Reson Med 2002;47:1202–1210.
9. Sodickson DK, Griswold MA, Jakob PM, Edelman RR, Manning WJ. Signal-to-noise ratio and signal-to-noise efficiency in SMASH imaging. Magn Reson Med 1999;41:1009–1022.
10. Griswold MA, Jakob PM, Nittka M, Goldfarb JW, Haase A. Partially parallel imaging with localized sensitivities (PILS). Magn Reson Med 2000;44:602–609.
11. Sodickson DK. Tailored SMASH image reconstructions for robust in vivo parallel MR imaging. Magn Reson Med 2000;44:243–251.
12. Bydder M, Larkman DJ, Hajnal JV. Generalized SMASH imaging. Magn Reson Med 2002;47:160–170.
13. Pruessmann KP, Weiger M, Börnert P, Boesiger P. Advances in sensitivity encoding with arbitrary *k*-space trajectories. Magn Reson Med 2001;46:638–651.
14. Kyriakos WE, Panych LP, Kacher DF, et al. Sensitivity profiles from an array of coils for encoding and reconstruction in parallel (SPACE RIP). Magn Reson Med 2000;44:301–308.
15. Tsao J, Boesiger P, Pruessmann KP. k-t BLAST and k-t SENSE: dynamic MRI with high frame rate exploiting spatiotemporal correlations. Magn Reson Med 2003;50:1031–1042.
16. Huang F, Akao J, Vijayakumar S, Duensing GR, Limkeman M. k-t GRAPPA: a *k*-space implementation for dynamic MRI with high reduction factor. Magn Reson Med 2005;54:1172–1184.
17. Hardy CJ, Darrow RD, Saranathan M, et al. Large field-of-view real-time MRI with a 32-channel system. Magn Reson Med 2004;52:878–884.
18. Fenchel M, Deshpande VS, Nael K, et al. Cardiac cine imaging at 3 tesla: initial experience with a 32-element body-array coil. Invest Radiol 2006;41:601–608.
19. Wiggins GC, Potthast A, Triantafyllou C, et al. A 96-channel MRI system with 23- and 90-channel phase array head coils at 1.5 tesla [Abstract]. Proc Int Soc Magn Reson Med 2005;13:671.
20. Bollenbeck J, Vester M, Oppelt R, Kroeckel H, Schnell W. A high performance multi-channel RF receiver for magnet resonance imaging systems [Abstract]. Proc Int Soc Magn Reson Med 2005;13:860.
21. Lin FH, Wald LL, Ahlfors SP, Hamalainen MS, Kwong KK, Belliveau JW. Dynamic magnetic resonance inverse imaging of human brain function. Magn Reson Med 2006;56:787–802.
22. Weiger M, Pruessmann KP, Boesiger P. 2D SENSE for faster 3D MRI. MAGMA 2002;14:10–19.
23. Dydak U, Weiger M, Pruessmann KP, Meier D, Boesiger P. Sensitivity-encoded spectroscopic imaging. Magn Reson Med 2001;46:713–722.
24. Sodickson DK, McKenzie CA. A generalized approach to parallel magnetic resonance imaging. Med Phys 2001;28:1629–1643.
25. Wang Y. Description of parallel imaging in MRI using multiple coils. Magn Reson Med 2000;44:495–499.
26. Jakob PM, Griswold MA, Edelman RR, Sodickson DK. AUTO-SMASH: a self-calibrating technique for SMASH imaging. MAGMA 1998;7:42–54.
27. Heidemann RM, Griswold MA, Haase A, Jakob PM. VD-AUTO-SMASH imaging. Magn Reson Med 2001;45:1066–1074.
28. Yeh EN, Stuber M, McKenzie CA, et al. Inherently self-calibrating non-Cartesian parallel imaging. Magn Reson Med 2005;54:1–8.
29. Heidemann RM, Griswold MA, Seiberlich N, et al. Direct parallel image reconstructions for spiral trajectories using GRAPPA. Magn Reson Med 2006;56:317–326.
30. Tsao J, Pruessmann KP, Boesiger P. Feedback regularization for SENSE reconstruction [Abstract]. Proc Int Soc Magn Reson Med 2002;10:739.
31. King KF, Angelos L. SENSE image quality improvement using matrix regularization [Abstract]. Proc Int Soc Magn Reson Med 2001;9:1771.
32. Liang ZP, Bammer R, Ji J, Pelc NJ, Glover GH. Making better SENSE: wavelet denoising, Tikhonov regularization, and total least squares [Abstract]. Proc Int Soc Magn Reson Med 2002;10:2388.
33. Katscher U, Manke D. Underdetermined SENSE using a-priori knowledge [Abstract]. Proc Int Soc Magn Reson Med 2002;10:2396.
34. Lin FH, Kwong KK, Belliveau JW, Wald LL. Parallel imaging reconstruction using automatic regularization. Magn Reson Med 2004;51:559–567.
35. Macovski A. Noise in MRI. Magn Reson Med 1996;36:494–497.
36. Pruessmann KP, Weiger M, Scheidegger MB, Boesiger P. SENSE: Sensitivity encoding for fast MRI. Magn Reson Med 1999;42:952–962.
37. Bydder M, Larkman DJ, Hajnal JV. Detection and elimination of motion artifacts by regeneration of *k*-space. Magn Reson Med 2002;47:677–686.
38. Bydder M, Atkinson D, Larkman DJ, Hill DL, Hajnal JV. Smash navigators. Magn Reson Med 2003;49:493–500.
39. Atkinson D, Larkman DJ, Batchelor PG, Hill DL, Hajnal JV. Coil-based artifact reduction. Magn Reson Med 2004;52:825–830.
40. Winkelmann R, Börnert P, Nehrke K, Doessel O. Efficient foldover suppression using sense. MAGMA 2005;18:63–68.
41. Winkelmann R, Börnert P, Doessel O. Ghost artifact removal using a parallel imaging approach. Magn Reson Med 2005;54:1002–1009.
42. Kellman P, McVeigh ER. Ghost artifact cancellation using phased array processing. Magn Reson Med 2001;46:335–343.
43. Kellman P, McVeigh ER. Phased array ghost elimination. NMR Biomed 2006;19:352–61.
44. Golay X, Pruessmann KP, Weiger M, et al. PRESTO-SENSE: an ultrafast whole-brain fMRI technique. Magn Reson Med 2000;43:779–786.
45. Lin FH, Huang TY, Chen NK, et al. Functional MRI using regularized parallel imaging acquisition. Magn Reson Med 2005;54:343–353.
46. Moeller S, Van de Moortele PF, Goerke U, Adriany G, Ugurbil K. Application of parallel imaging to fMRI at 7 tesla utilizing a high 1D reduction factor. Magn Reson Med 2006;56:118–129.
47. Lutcke H, Merboldt KD, Frahm J. The cost of parallel imaging in functional MRI of the human brain. Magn Reson Imaging 2006;24:1–5.
48. Dickerson B. Functional magnetic resonance imaging. Neurotherapeutics 2007;00:000–000 (this issue).
49. Alexander A. Diffusion tensor imaging of the brain. Neurotherapeutics 2007;00:000–000 (this issue).
50. Maier S. Diffusion tensor imaging of the spinal cord. Neurotherapeutics 2007;00:000–000 (this issue).
51. Bammer R, Keeling SL, Augustin M, et al. Improved diffusion-weighted single-shot echo-planar imaging (EPI) in stroke using sensitivity encoding (SENSE). Magn Reson Med 2001;46:548–554.
52. Augustin M, Fazekas F, Bammer R. Fast patient workup in acute stroke using parallel imaging. Top Magn Reson Imaging 2004;15:207–219.

53. Naganawa S, Koshikawa T, Kawai H, et al. Optimization of diffusion-tensor MR imaging data acquisition parameters for brain fiber tracking using parallel imaging at 3 T. Eur Radiol 2004;14:234–238.
54. Tsuchiya K, Fujikawa A, Suzuki Y. Diffusion tractography of the cervical spinal cord by using parallel imaging. AJNR Am J Neuroradiol 2005;26:398–400.
55. Tsuchiya K, Fujikawa A, Tateishi H, Nitatori T. Visualization of cervical nerve roots and their distal nerve fibers by diffusion-weighted scanning using parallel imaging. Acta Radiol 2006;47:599–602.
56. Dydak U, Weiger M, Pruessmann KP, Meier D, Boesiger P. Sensitivity-encoded spectroscopic imaging. Magn Reson Med 2001;46:713–722.
57. Golay X, Gillen J, van Zijl PC, Barker PB. Scan time reduction in proton magnetic resonance spectroscopic imaging of the human brain. Magn Reson Med 2002;47:384–387.
58. Lin FH, Tsai SY, Otazo R, et al. Sensitivity-encoded (SENSE) proton echo-planar spectroscopic imaging (PEPSI) in the human brain. Magn Reson Med 2007;57:249–257.
59. Lenkinski B. Magnetic resonance imaging spectroscopy. Neurotherapeutics 2007;00:000–000 (this issue).
60. Jakob PM, Griswold MA, Edelman RR, Manning WJ, Sodickson DK. Accelerated cardiac imaging using the SMASH technique. J Cardiovasc Magn Reson 1999;1:153–157.
61. Tsao J, Kozerke S, Boesiger P, Pruessmann KP. Optimizing spatiotemporal sampling for k-t BLAST and k-t SENSE: application to high-resolution real-time cardiac steady-state free precession. Magn Reson Med 2005;53:1372–1382.
62. Wintersperger BJ, Reeder SB, Nikolaou K, et al. Cardiac CINE MR imaging with a 32-channel cardiac coil and parallel imaging: impact of acceleration factors on image quality and volumetric accuracy. J Magn Reson Imaging 2006;23:222–227.
63. Park J, Larson AC, Zhang Q, Simonetti O, Li D. High-resolution steady-state free precession coronary magnetic resonance angiography within a breath-hold: parallel imaging with extended cardiac data acquisition. Magn Reson Med 2005;54:1100–1106.
64. Nehrke K, Börnert P, Mazurkewitz P, Winkelmann R, Graesslin I. Free-breathing whole-heart coronary MR angiography on a clinical scanner in four minutes. J Magn Reson Imaging 2006;23:752–756.
65. Weiger M, Pruessmann KP, Kassner A, et al. Contrast-enhanced 3D MRA using SENSE. J Magn Reson Imaging. 2000;12:671–677.
66. Lin J, Chen B, Wang JH, Zeng MS, Wang YX. Whole-body three-dimensional contrast-enhanced magnetic resonance (MR) angiography with parallel imaging techniques on a multichannel MR system for the detection of various systemic arterial diseases. Heart Vessels 2006;21:395–398.
67. Nikolaou K, Kramer H, Grosse C, et al. High-spatial-resolution multistation MR angiography with parallel imaging and blood pool contrast agent: initial experience. Radiology 2006;241:861–872.
68. Zech CJ, Herrmann KA, Huber A, et al. High-resolution MR-imaging of the liver with T2-weighted sequences using integrated parallel imaging: comparison of prospective motion correction and respiratory triggering. J Magn Reson Imaging 2004;20:443–450.
69. Winkelmann R, Börnert P, De Becker J, Hoogeveen R, Mazurkewitz P, Dössel O. Dual-contrast single breath-hold 3D abdominal MR imaging. MAGMA 2006;19:297–304.
70. Bottomley PA, Andrew ER. RF magnetic field penetration, phase shift and power dissipation in biological tissue: implications for NMR imaging. Phys Med Biol 1978;23:630–43.
71. Röschmann P. Radiofrequency penetration and absorption in the human body: limitations to high-field whole-body nuclear magnetic resonance imaging. Med Phys 1987;14:922–31.
72. Vaughan T. Ultra-high-field magnetic resonance imaging neuroimaging. Neurotherapeutics 2007;00:000–000 (this issue).
73. Sotgiu A, Hyde JS. High-order coils as transmitters for NMR imaging. Magn Reson Med 1986;3:55–62.
74. Ibrahim TS, Lee R, Baertlein BA, Kangarlu A, Robitaille PL. Application of finite difference time domain method for the design of birdcage RF head coils using multi-port excitations. Magn Reson Imaging 2000;18:733–742.
75. Seifert F, Rinneberg H. Adaptive coil control: SNR optimization of a TR volume coil for single voxel MRS at 3 T [Abstract]. Proc Int Soc Magn Reson Med 2002;10:162.
76. Adriany G, Van de Moortele PF, Wiesinger F, et al. Transmit and receive transmission line arrays for 7 tesla parallel imaging. Magn Reson Med 2005;53:434–445.
77. Zhu Y, Giaquinto R. Improving flip angle uniformity with parallel excitation [Abstract]. Proc Int Soc Magn Reson Med 2005;13:2752.
78. Ullmann P, Junge S, Wick M, Seifert F, Ruhm W, Hennig J. Experimental analysis of parallel excitation using dedicated coil setups and simultaneous RF transmission on multiple channels. Magn Reson Med 2005;54:994–1001.
79. Pauly J, Nishimura D, Macovski A. A *k*-space analysis of small-tip-angle excitation. J Magn Reson 1989;81:43–56.
80. Börnert P, Aldefeld B. On spatially selective RF excitation and its analogy with spiral MR image acquisition. MAGMA 1998;7:166–178.
81. Katscher U, Börnert P, Leussler C, van den Brink J. Transmit SENSE. Magn Reson Med 2003;49:144–150.
82. Zhu Y. Parallel excitation with an array of transmit coils. Magn Reson Med 2004;51:775–784.
83. Hardy VJ, Cline HE. Spatial localization in two dimensions using NMR designer pulses. J Magn Reson 1989;82:647–654.
84. Bottomley PA, Hardy CJ. Progress in efficient 3-dimensional spatially localized in vivo P-31 NMR-spectroscopy using multi-dimensional spatially selective (Rho) pulses. J Magn Reson 1987;74:550–556.
85. Börnert P, Schäffter T. Curved slice imaging. Magn Reson Med 1996;36:932–939.
86. Sachs TS, Meyer CH, Hu BS, Kohli J, Nishimura D, Macovski A. Real-time motion detection in spiral MRI using navigators. Magn Reson Med 1994;32:639–645.
87. Pauly JM, Hu BS, Wang SJ, Nishimura DG, Marcovski A. A three-dimensional spin-echo or inversion pulse. Magn Reson Med 1993;29:2–6.
88. Wong ST, Roos MS. A strategy for sampling on a sphere applied to 3D selective RF pulse design. Magn Reson Med 1994;32:778–784.
89. Saekho S, Boada FE, Noll DC, Stenger VA. Small tip angle three-dimensional tailored radiofrequency slab-select pulse for reduced B1 inhomogeneity at 3 T. Magn Reson Med 2005;53:479–484.
90. Ulloa JL, Irarrazaval P, Hajnal JV. Exploring 3D RF shimming for slice selective imaging [Abstract]. Proc Int Soc Magn Reson Med 2005;13:21.
91. Glover GH, Hayes CE, Pelc NJ, et al. Comparison of linear and circular polarization for magnetic resonance imaging. J Magn Reson 1985;64:255–270.
92. Barker GJ, Simmons A, Arridge SR, Tofts PS. A simple method for investigating the effects of non-uniformity of radiofrequency transmission and radiofrequency reception in MRI. Br J Radiol 1998;71:59–67.
93. Griswold MA, Kannengiesser S, Müller M, Jakob PM. Autocalibrated accelerated parallel excitation (Transmit-GRAPPA) [Abstract]. Proc Int Soc Magn Reson Med 2005;13:2435.
94. Pauly J, Nishimura D, Macovski A. A linear class of large-tip-angle selective excitation pulses. J Magn Reson 1989;82:571–587.
95. Grissom W, Yip CY, Zhang Z, Stenger VA, Fessler JA, Noll DC. Spatial domain method for the design of RF pulses in multicoil parallel excitation. Magn Reson Med 2006;56:620–629.
96. Yip CY, Fessler JA, Noll DC. A novel, fast and adaptive trajectory in three-dimensional excitation *k*-space [Abstract]. Proc Int Soc Magn Reson Med 2005;13:2350.
97. Conolly S, Nishimura DG, Macovski A, Glover G. Variable-rate selective excitation. J Magn Reson 1988;78:440–458.
98. Graesslin I, Niemann M, Harvey P, Vernickel P, Katscher U. SAR and RF power reduction with parallel excitation using non-Cartesian trajectories [Abstract]. MAGMA 2005;18:S251.

99. Katscher U, Börnert P, van den Brink, JS. Theoretical and numerical aspects of Transmit SENSE. IEEE Trans Med Imaging 2004;23:520–525.
100. Yip CY, Fessler JA, Noll DC. Iterative RF pulse design for multidimensional, small-tip-angle selective excitation. Magn Reson Med 2005;54:908–917.
101. Saekho S, Boada FE, Noll DC, Stenger VA. Small tip angle three-dimensional tailored radiofrequency slab-select pulse for reduced B1 inhomogeneity at 3 T. Magn Reson Med 2005;53: 479–484.
102. Boskamp E, Lee RF. Whole body LPSA tranceive array [Abstract]. Proc Int Soc Magn Reson Med 2002;10:903.
103. Weyers D, Boskamp E. An 8 channel volume transmit coil [Abstract]. Proc Int Soc Magn Reson Med 2002;10:901.
104. Lee RF, Giaquinto RO, Hardy CJ. Coupling and decoupling theory and its application to the MRI phased array. Magn Reson Med 2002;48:203–213.
105. Vernickel P, Röschmann P, Findeklee C, et al. An eight channel transmit/receive body coil for 3T [Abstract]. Proc Int Soc Magn Reson Med 2006;14:123.
106. Zhu Y, Watkins R, Giaquinto R, et al. Parallel excitation on an eight transmit-channel MRI system [Abstract]. Proc Int Soc Magn Reson Med 2005;13:14.
107. Graesslin I, Vernickel P, Schmidt J, et al. Whole body 3T MRI system with eight parallel rf transmission channels [Abstract]. Proc Int Soc Magn Reson Med 2006;14:129.
108. Setsompop K, Wald LL, Alagappan V, et al. Parallel RF transmission with eight channels at 3 tesla. Magn Reson Med 2006; 56:1163–1171.
109. Katscher U, Röhrs J, Börnert P. Basic considerations on the impact of the coil array on the performance of Transmit SENSE. MAGMA 2005;18:81–88.
110. Zhu Y. RF power deposition and "g-factor" in parallel transmit [Abstract]. Proc Int Soc Magn Reson Med 2006;14:599.
111. Katscher U, Vernickel P, Overweg J. Basics of RF power behaviour in parallel transmission [Abstract]. Proc Int Soc Magn Reson Med 2005;13:17.
112. Graesslin I, Falaggis K, Vernickel P, et al. Safety considerations concerning SAR during RF amplifier malfunctions in parallel transmission [Abstract]. Proc Int Soc Magn Reson Med 2006;14:2041.